THE ASTROPHYSICAL JOURNAL, 449:28–41, 1995 August 10

THEORY OF EXPLORING THE DARK HALO WITH MICROLENSING. I. POWER-LAW MODELS

C. ALCOCK,[1,2] R. A. ALLSMAN,[3] T. S. AXELROD,[3] D. P. BENNETT,[1,2] K. H. COOK,[1,2] N. W. EVANS,[4]
K. C. FREEMAN,[3] K. GRIEST,[2,5] J. JIJINA,[5] M. LEHNER,[5] S. L. MARSHALL,[2,6] S. PERLMUTTER,[2]
B. A. PETERSON,[3] M. R. PRATT,[2,6] P. J. QUINN,[3] A. W. RODGERS,[3]
C. W. STUBBS,[2,6] AND W. SUTHERLAND[7]
(THE MACHO COLLABORATION)
Received 1994 November 9; accepted 1995 February 16

ABSTRACT

If microlensing of stars by dark matter has been detected, then the way is open for the development of new methods in galactic astronomy. This series of papers investigates what microlensing can teach us about the structure and shape of the dark halo. In this paper we present formulae for the microlensing rate, optical depth, and event duration distributions for a simple set of axisymmetric disk-halo models. The halos are based on the "power-law models" of Evans which have simple velocity distributions.

Using these models, we show that there is a large uncertainty in the predicted microlensing rate because of uncertainty in the halo parameters. For example, models which reproduce the measured galactic observables to within their errors still differ in microlensing rate toward the Magellanic Clouds by more than a factor of 10. We find that while the more easily computed optical depth correlates well with microlensing rate, the ratio of optical depth to rate can vary by a factor of 2 (or greater if the disk is maximal). Comparison of microlensing rates toward the Large and Small Magellanic Clouds (LMC and SMC) and M31 can be used to aid determinations of the halo flattening and rotation curve slope. For example, the ratio of microlensing rates toward the LMC and SMC is $\sim$0.7–0.8 for E0 halos and $\sim$1.0–1.2 for E7 halos. Once the flattening has been established, the ratio of microlensing rates toward M31 and the LMC may help to distinguish between models with rising, flat, or falling rotation curves. Comparison of rates along LMC and galactic bulge lines of sight gives useful information on the halo core radius, although this may not be so easy to extract in practice. Maximal disk models provide substantially smaller halo optical depths, shorter event durations, and even larger model uncertainties.

Subject headings: dark matter — galaxies: halos — Galaxy: structure — gravitational lensing

1. INTRODUCTION

The recent detection of possible gravitational microlensing events (Alcock et al. 1993; Aubourg et al. 1993; Udalski et al. 1993, Alcock et al. 1995; Udalski et al. 1994a, b) gives hope that at least part of the dark matter content of our Galaxy is directly accessible to observation. The dark halo, whose extent has been studied gravitationally for many years via velocities of stars, gas, and satellites (e.g., Fich & Tremaine 1991), contains at least 3 times (and perhaps more than 10 times) the mass of the luminous Galaxy. Its identity is one of the major unsolved problems in astronomy (e.g., Ashman 1992; Primack, Seckel, & Sadoulet 1988). While it is possible that the halo consists mostly of exotic nonbaryonic elementary particles, the idea of Paczyński (1986) of searching for massive compact halo objects (MACHOs) in the range $10^{-8}\,M_\odot$ to $10^{3}\,M_\odot$ by monitoring millions of stars in the LMC may have borne fruit in the experimental programs.

If the Milky Way halo contains large numbers of MACHOs, then the gravitational microlensing experiments now underway should have the potential to determine the number and distribution of MACHOs in the halo, as well as their mass distribution. The next step for the microlensing experiments will be to gather more events and then translate the number and duration of those events into an estimate of the mass fraction f of the dark halo which consists of MACHOs in the relevant mass range. To accomplish this goal, a model of the dark halo is necessary. In the past, simple spherical models with flat rotation curves have been considered (Paczyński 1986; Griest 1991; DeRujula, Jetzer, & Masso 1991; Nemiroff 1991). These have been valuable in estimating the order-of-magnitude effects but suffer from at least three important deficiencies:

1. The halo may not be spherical. N-body simulations of gravitational collapse of collisionless dark matter generically produce axisymmetric or triaxial halos (Warren et al. 1992; Dubinski & Carlberg 1991; Katz 1991). The recent papers of Sackett & Gould (1993), Frieman & Scoccimarro (1994), and Jetzer & Masso (1994), have made an important start on the study of microlensing effects in flattened halos.

2. The effect of the Galactic disk is ignored. The disk makes a significant contribution to the local circular speed. Modeling without proper allowance for this effect leads us to overesti-

[1] Lawrence Livermore National Laboratory, Livermore, CA 94550.
[2] Center for Particle Astrophysics, University of California, Berkeley, CA 94720.
[3] Mount Stromlo and Siding Spring Observatories, Australian National University, Weston, ACT 2611, Australia.
[4] Theoretical Physics, Department of Physics, University of Oxford, Oxford, England OX1 3NP, UK.
[5] Department of Physics, University of California, San Diego, CA 92093.
[6] Department of Physics, University of California, Santa Barbara, CA 93106.
[7] Astrophysics, Department of Physics, University of Oxford, Oxford, England OX1 3RH, UK.

mate the gravity field and hence the mass of the dark halo. That is, since the amount of material in the Galactic halo is set by the local circular speed, a larger contribution to this speed by the disk means a smaller halo is needed to explain the total circular velocity.

3. It is only a simplified view of the data that permits one to regard the rotation curve of the Milky Way as flat. In fact, even the sign of the local gradient of the rotation law at the Sun is not known—Fich, Blitz, & Stark (1989) estimate that it may be rising or falling by about 30 km s^{-1} outward from the solar circle to a galactocentric radius of 17 kpc.

In this paper, we make a start toward quantifying and remedying these defects by calculating the microlensing rate and optical depth in a set of simple, flexible, and realistic halo models. We take the power-law models (Evans 1993, 1994, hereafter E93, E94)—for which simple and self-consistent distribution functions are known—and provide an approximate method to allow for the influence of the Galactic disk. This enables calculation not just of the optical depth, but also the event rate and the distribution of even durations. In this paper, the emphasis is on the uncertainties in microlensing predictions and what can be done to reduce them. Since there are many possible models of the dark halo consistent with current observations, there is a substantial scatter in the predicted microlensing rate, and this in turn contributes to an uncertainty in the measurement of the fraction of the halo consisting of MACHOs. Of course, this is directly relevant to the difficult but important question of whether the observed microlensing rates can rule out or support the existence of nonbaryonic matter in the halo.

We show that the often-calculated optical depth is a useful predictor of the microlensing rate to a factor of ~ 2. For more accurate work and to predict event durations, a distribution of MACHO velocities is needed. By considering a large range of model parameters consistent with observations, we find the microlensing optical depth can vary by a factor of 6 or more. If the disk of the Milky Way is "maximal"—in the sense that it provides almost all the Galactocentric acceleration—then a much smaller halo is required. This gives an even larger spread in predicted optical depth, rate, and event durations. An attractive possibility is to use the measured microlensing rates toward different sources (e.g., LMC, SMC, M31, and the Galactic bulge) to determine some of the halo and disk parameters, thereby providing a new tool for the study of galactic structure and at the same time reducing the halo uncertainty in the measurement of f. We corroborate the Sackett & Gould (1993) prediction that the ratio of LMC to SMC optical depth is a robust indicator of the flattening of the dark halo—and extend it by showing that the ratio of microlensing rate distinguishes flatness as well. We predict that the ratio of rates toward M31 and the LMC may enable us to discover whether the rotation curve is rising or falling (or, equivalently, the extent of the dark halo). A comparison of the bulge and LMC rates can provide information on the halo core radius.

The plan of the paper is as follows: In § 2 we review the axisymmetric models and present formulas for the optical depth, microlensing rate, and event durations. In § 3 we discuss the halo parameters and their allowed range and explain how to take into account the effect of the Galactic disk. In § 4 we compare optical depth and rate and discuss the uncertainties in microlensing rates due to uncertainties in the parameters. In § 5 we discuss reducing those uncertainties by comparing results along different lines of sight, in § 6 we discuss distributions of event durations, and in § 7 we summarize our conclusions.

2. AXISYMMETRIC MODELS

The primary goal of the galactic gravitational microlensing experiments is to determine the mass of the dark halo in MACHOs. The experiments search for MACHOs by monitoring millions of stars nightly in the Large Magellanic Cloud (LMC), the Small Magellanic Cloud (SMC), the Galactic bulge, and perhaps in the future in the M31 galaxy (Crotts 1992; Baillon et al. 1993). If the dark halo contains large numbers of MACHOs, occasionally one passes close to the observer-star line of sight and acts as a gravitational lens, causing a time-dependent magnification of the stellar image. The resulting light curve is determined by only a few quantities such as the distance s from us to the MACHO, MACHO mass m, MACHO transverse velocity $v_\perp$, and impact parameter b. The magnification $A(t)$ as a function of time t is given by

$$\begin{aligned} A(t) &= (u^2+2)/[u(u^2+4)^{1/2}] , \\ u(t) &= b/R_e = [u_{\min}^2 + \omega^2(t-t_0)^2]^{1/2} , \\ R_e &= (2/c)[Gms(1-s/L)]^{1/2} , \end{aligned} \tag{1}$$

where the peak magnification $A_{\max}$ is given by inverting $u_{\min} = u(A_{\max})$, $\omega = v_\perp/R_e$, and L is the distance to the star. Experimentally, microlensing events are characterized by the maximum magnification $A_{\max}$, the time of the peak t_0, and the duration of the event $\hat{t}$, where $\hat{t} = 2/\omega$. Also used in the literature as an "event duration" is $t_e = \hat{t}(u_T^2 - u_{\min}^2)^{1/2}$. This is time for which $A \geq A_T$, with $A_T = A(u_T)$. Using $A_T = 1.34$ corresponds to $u_T = 1$, which is the time inside the Einstein radius R_e. A more thorough discussion can be found in Paczyński (1986) and Griest (1991).

An observing team measures the number and duration of microlensing events. The number of observed events is proportional to the number of stars monitored, the duration of the experiment, the experimental efficiency, and the rate at which microlensing occurs. The primary observables are the optical depth τ, the rate Γ, and the average duration of the events $\langle \hat{t} \rangle$. They are related by

$$\tau = \Gamma \langle t_e \rangle = \frac{\pi}{4} \Gamma \langle \hat{t} \rangle . \tag{2}$$

If the distribution of MACHO masses $n(m)$ were a delta function, then Γ would be $\Gamma = \Gamma_1 (m/M_\odot)^{-1/2}$, where Γ_1 is the rate with $m = M_\odot$ and is independent of mass. For a general normalized mass distribution, $\Gamma = \eta_m \Gamma_1$, where the mass integral is

$$\eta_m = \int dm\, n(m) (m/M_\odot)^{-1/2} . \tag{3}$$

This also implies that $\langle \hat{t} \rangle = \langle \hat{t} \rangle_1 \eta_m^{-1}$.

The optical depth is the number of MACHOs inside the microlensing tube with radius $u_T R_e(s)$ and length L. It depends only on the density of MACHOs ρ:

$$\tau = \int \frac{\rho(x)}{m} \pi u_T^2 R_e^2(s) ds . \tag{4}$$

Unlike the rate or average duration, it is independent of the MACHO mass distribution. For this reason, it also contains no direct information about the mass of the lensed objects. Note also that since detection efficiencies depend upon the

duration of events, it is important to have models which predict durations. Now to find the rate at which MACHOs enter the microlensing tube requires knowledge of the distribution of velocities all along the tube. So the rate and the distribution of event durations are hard to calculate, because they require the entire phase space distribution function (DF) $F(\boldsymbol{v}, \boldsymbol{x})$. The differential rate is given by

$$d\Gamma = \frac{1}{m} F(\boldsymbol{v}, \boldsymbol{x}) \cos\theta u_T R_e v_\perp d^3v\, dx\, d\alpha\,, \tag{5}$$

where the angles and notation are defined in Griest (1991).

What makes the calculation particularly difficult is that the DF cannot be prescribed arbitrarily as a Maxwellian, for instance. This is because the MACHOs are collisionless, so the DF is constrained to obey the collisionless Boltzmann equation. By Jeans's theorem, this implies that the DF depends only on the isolating integrals of motion (see Binney & Tremaine 1987, p. 220). Self-consistent solutions for distributions of velocities that build flattened halo models are scarce. The largest known set of axisymmetric models with simple DFs comprises the "power-law galaxies" (E93, E94). These form the basis for the exploration of microlensing in this paper, allowing us to go beyond simple spherical models. Note, however, that all these models are axisymmetric and oblate, while N-body simulations suggest that halos may well be triaxial. Exploration of triaxial models will be done in a future paper.

The parameters of the power-law models are as follows:

1. The core radius R_c, which measures the scale at which the density law begins to soften.
2. The flattening parameter q, which is the axis ratio of the concentric equipotential spheroids, with $q = 1$ representing a spherical (E0) halo and $q \sim 0.7$ representing an ellipticity of about E6. The "isophotal" ellipticity of the dark halo is a function of q, as well as other parameters of the model (see E94, eq. [2.9]).
3. The parameter β, which determines whether the rotation curve asymptotically rises, falls or is flat. At large distances R in the equatorial plane, the rotation velocity $v_{\rm circ} \sim R^{-\beta}$. So $\beta = 0$ corresponds to a flat rotation curve, while $\beta < 0$ is a rising rotation curve and $\beta > 0$ is falling.
4. The solar radius R_0, which is the distance of the Sun from the Galactic center.
5. Finally, the normalization velocity v_0, which determines the overall depth of the potential well and hence the typical velocities of MACHOs in the halo. In the limit $\beta = 0$, $q = 1$ and large R (spherical halo with a flat rotation curve) $v_0 = v_{\rm circ}$.

Using z as the height above the equatorial plane, the potential of the power-law models is

$$\Psi = \begin{cases} \dfrac{v_0^2 R_c^\beta/\beta}{(R_c^2 + R^2 + z^2 q^{-2})^{\beta/2}}\,, & \text{if } \beta \neq 0\,, \\ -\dfrac{v_0^2}{2} \log (R_c^2 + R^2 + z^2 q^{-2})\,, & \text{if } \beta = 0\,, \end{cases} \tag{6}$$

and the mass density is

$$\rho = \frac{v_0^2 R_c^\beta}{4\pi G q^2} \frac{R_c^2(1+2q^2) + R^2(1-\beta q^2) + z^2[2-(1+\beta)q^{-2}]}{(R_c^2 + R^2 + z^2 q^{-2})^{(\beta+4)/2}}\,. \tag{7}$$

The DF corresponding to this potential-density pair is

$$F(E, L_z) = \begin{cases} AL_z^2 |E|^{4/\beta - 3/2} + B|E|^{4/\beta - 1/2} \\ \quad + C|E|^{2/\beta - 1/2}\,, & \text{if } \beta \neq 0\,, \\ AL_z^2 \exp(4E/v_0^2) + B \exp(4E/v_0^2) \\ \quad + C \exp(2E/v_0^2)\,, & \text{if } \beta = 0\,, \end{cases} \tag{8}$$

where the constants A, B, and C are given in E93 and E94. As required by Jeans's theorem, the DFs depend only on the isolating integrals of motion, namely the relative energy per unit mass $E = \Psi - \frac{1}{2}v^2$, and the angular momentum per unit mass about the symmetry axis L_z. The circular velocity in the equatorial plane is

$$v_{\rm circ}^2 = \frac{v_0^2 R_c^\beta R^2}{(R_c^2 + R^2)^{(\beta+2)/2}}\,. \tag{9}$$

Note that the limit $q = 1$, $\beta = 0$, and $R_c = 0$ recovers the standard singular isothermal sphere used by Paczyński. Allowing a core radius gives

$$\rho = \frac{v_0^2}{4\pi G} \frac{r^2 + 3R_c^2}{(r^2 + R_c^2)^2}\,, \tag{10}$$

where $r^2 = R^2 + z^2$. This differs from the cored isothermal sphere considered by Griest (1991) in several ways. First, the rotation curve approaches its asymptotic value more quickly. Second, the DF given by the $q = 1$, $\beta = 0$ limit of equation (8) is self-consistent, whereas Griest (1991) assumed an approximate Maxwellian distribution of velocities.

So far we have only modeled the dark halo. However, in the standard model, a substantial fraction ($\sim$40%) of the centripetal force at the solar radius derives from the disk stars. This is represented by a thin exponential disk with a scale length of $R_d = 3.5$ kpc, normalized to a surface density of $\Sigma_0 = 50\ M_\odot\ {\rm pc}^{-2}$ at the solar radius (Gilmore, Wyse, & Kuijken 1989; Gould 1990). It is possible that the disk of our Galaxy is substantially larger than the canonical value (Oort 1960; Bahcall 1984; Kuijken & Gilmore 1989; Gould 1990). Recent microlensing results (Alcock et al. 1994; Udalski et al. 1994), as well as studies of the optical rotation curves of external galaxies (Buchhorn 1992; Kent 1992), may suggest this. We consider such a "maximal disk" by taking $\Sigma_0 = 100\ M_\odot\ {\rm pc}^{-2}$. This value of column density is somewhat higher than the value $\Sigma_0 \simeq 90\ M_\odot\ {\rm pc}^{-2}$ found by Oort (1960), and the value $\Sigma_0 \simeq 75\ M_\odot\ {\rm pc}^{-2}$ found by Bahcall (1984) and Kuijken & Gilmore (1991). The values of Σ_0 quoted here are local dynamical measurements from the velocities and positions of tracer stars above the Galactic plane near the solar circle. They thus measure the total mass column (stars, gas, white dwarfs, and disk dark matter). If we take the assumed exponential form of the disk column density to be a precise prediction for the local column density, then the bulk of this "maximal disk" could not consist of stars with a standard mass function, since estimates of the local column density in stars (from star counts) are much lower (Bahcall 1984). Also Paczyński et al. (1994) have argued that star counts toward the bulge are probably lower than predicted for such a massive disk and a standard mass and luminosity function. Also note that while we are investigating the effect of a maximal disk on halo microlensing, others have proposed that the bulge microlensing results are due to a "bar" in the Milky Way (Zhao, Spergel, & Rich 1995; Paczyński et al. 1994). Models with a canonical disk plus bar would probably have halo microlensing rates similar to our maximal disk models.

Given either the canonical or maximal value for Σ_0, the rotation velocity added in quadrature is thus (Freeman 1970; Binney & Tremaine 1987, p. 77)

$$v_{\rm disk}^2 = 4\pi G\Sigma_0 R_d e^{R_0/R_d} y^2[I_0(y)K_0(y) - I_1(y)K_1(y)] , \quad (11)$$

where $y = R/(2R_d)$, and I_n and K_n are modified Bessel functions. Note that in adding a contribution from the disk to the local circular velocity, we have sacrificed self-consistency. We should find the DF of the power-law halo in the combined potential field of both disk and halo—instead, we use the DF (8). As has been argued elsewhere (Evans & Jijina 1994), this is a reasonable approximation for the LMC, SMC, and M31, where microlensing typically occurs at heights above the equatorial plane of many kiloparsecs.

In this paper, our aim is to estimate the contribution of the Galactic halo to microlensing. Of course, this is not the only possible source of deflectors. Toward the LMC, there is the possibility of microlensing by the LMC dark halo or disk (Gould 1993b; Sahu 1994). The optical depth is $\sim 2.5 \times 10^{-7}$ for microlensing by LMC halo lenses and $\sim 0.09 \times 10^{-7}$ for LMC disk lenses. The Galactic halo makes a contribution that is roughly 3 times greater and so is the dominant source of lenses. However, this is not the case for lines of sight toward M31. The optical depth is dominated by MACHOs in the halo and disk of M31 (Crotts 1992; Gould 1993a). Crotts (1992) estimates that the halo of our own Galaxy contributes just 20% to the total optical depth. Microlensing toward the Galactic bulge poses perhaps the hardest problem of separating the contributions of different deflector populations. Bulge stars can undergo microlensing not only by halo MACHOs, but also by other bulge and disk stars (Griest et al. 1991; Paczyński 1991; Kiraga & Paczyński 1994). At Baade's window, the optical depth is $\sim 6.3 \times 10^{-7}$ for microlensing by bulge lenses and $\sim 5.0 \times 10^{-7}$ for disk lenses. The dark halo only makes an important contribution if the core radius is small.

We are now in a position to calculate the microlensing observables—the optical depth, rate, and average duration of events. They can be found using equations (2), (3), (4), and (7). The results are single quadratures and readily evaluated on the computer. They are displayed in Appendix A. In Appendix B, we give the differential microlensing rate $d\Gamma/d\hat{t}$, where $\hat{t}$ is defined just after equation (1). The probability of obtaining an event of duration $\hat{t}$ is just $(d\Gamma/d\hat{t})/\Gamma$.

3. RANGE OF MODELS

In order to explore the scatter in microlensing observables, we build a set of halo models which span the observationally allowed range. The power-law galaxy models allow us to vary the flattening, core radius, and rotation law, and we consider both canonical and maximal disks. For each parameter in the model, we therefore find the range permitted by the observations. Then, several values of each parameter are chosen to represent the range. We also ensure that each set of parameters gives a model consistent with the measured Milky Way rotation curve. Therefore, we study the statistical properties of an ensemble of models, each of which is a plausible representation of the dark halo of the Milky Way.

For the dark halo flattening, little is known. So the entire range of flattening allowed by the power-law models is examined. This varies between E0 or spherical ($q = 1$) and roughly E6 or E7 (depending on β). The core radius of the dark halo is also uncertain—Bahcall, Schmidt, & Soneria (1983) estimate R_c as 2 kpc from star count data, while Caldwell & Ostriker (1981) suggest 10 kpc. If the disk is maximal, values as large as 20 kpc are possible. We consider values of 2 kpc, 5 kpc, 10 kpc, and 20 kpc. The parameter β determines the slope of asymptotic circular velocity. Between R_0 and $2R_0$, the circular velocity is probably within 10%–15% of the IAU value of 220 km s^{-1}, but whether the measured H I rotational velocities rise or fall with R depends upon estimates of the solar position R_0 and the local circular speed $v_{\rm circ}(R_0)$ (see Fich et al. 1989; Jones et al. 1993). Beyond 20 kpc, little is known directly, though arguments based on the kinematics of distant satellite galaxies support the idea of a relatively flat rotation curve out to an unknown cutoff (Fich & Tremaine 1991). However, current theories of galaxy formation tend to favor the alternative view that dark halos extend indefinitely, fading into structure on larger scales. Therefore, we do not consider a halo cutoff in this paper—it would add yet another poorly known parameter to our model. We investigate power-law halos with $\beta = -0.2$, 0, and 0.2. These correspond to rotation curves which rise by $\sim 15\%$, are flat, or fall by $\sim 15\%$ between the solar radius and twice the solar radius, depending a little upon R_c.

The value of the solar radius R_0 has been reviewed by Reid (1989). He shows that most recent determinations lie between 7 kpc and 9 kpc, with 7.7 kpc being his preferred value. This differs considerably from the IAU value of 8.5 kpc (Kerr & Lynden-Bell 1986). We examine the values $R_0 = 7$, 8, and 9 kpc. Finally, perhaps the single most important parameter is the normalization velocity v_0. Given our fixed disk contribution to the total rotation law, the parameter v_0 is now specified once we settle upon a choice for $v_{\rm circ}(R_0)$. Merrifield (1992) estimates $v_{\rm circ}(R_0) = 200 \pm 10$ km s^{-1} Fich et al. (1989) give $v_{\rm circ}(R_0) = 220 \pm 30$ km s^{-1}, while Rohlfs et al. (1986) gives values between 170 and 200 km s^{-1} between $R_0 = 6$ kpc and $R_0 = 16$ kpc. For our ensemble of models, we impose the constraint that the total circular velocity lies between 180 and 250 km s^{-1} at R_0 and $2R_0$. Note that the IAU value is 220 km s^{-1} (Kerr & Lynden-Bell 1986). We also investigated a more restricted ensemble of models with $190 \le v_{\rm circ}(R_0) \le 230$ km s^{-1}. We find all our results also hold for this more restricted ensemble.

4. UNCERTAINTIES IN THE RATES

First, let us consider the difference caused by using the optical depth instead of the microlensing event rate. The optical depth to microlensing is the mean number of MACHOs in the microlensing tube; that is the number of microlensing events taking place at a given moment. It is easy to calculate since it is independent of lens mass and velocity and only requires knowledge of the density distribution $\rho(x)$. For this reason, it is the most widely estimated quantity. But how well does it trace the microlensing rate?

We are able to answer this question since both the rate Γ (eq. [A1]) and the optical depth τ(eq. [A6]) are known for the power-law models. One way to test this is to plot $\langle\hat{t}\rangle$, which is the ratio of optical depth τ and Γ, $\langle\hat{t}\rangle = (4/\pi)\tau/\Gamma$, for many different models. The average duration $\langle\hat{t}\rangle$ is a constant if τ and Γ are well correlated. In Figure 1, we show histograms of $\langle\hat{t}\rangle$ for microlensing toward the LMC, SMC, and M31 for our ensemble of models. Figures 1*a*–1*c* demonstrate that $\langle\hat{t}\rangle$ tends to vary by more than a factor of 2 between models. Figures 1*d*–1*f* show an even larger spread for maximal disk models. Figures 2*a*–2*f* show this another way by plotting the rate versus the optical depth for the set of models. These plots show

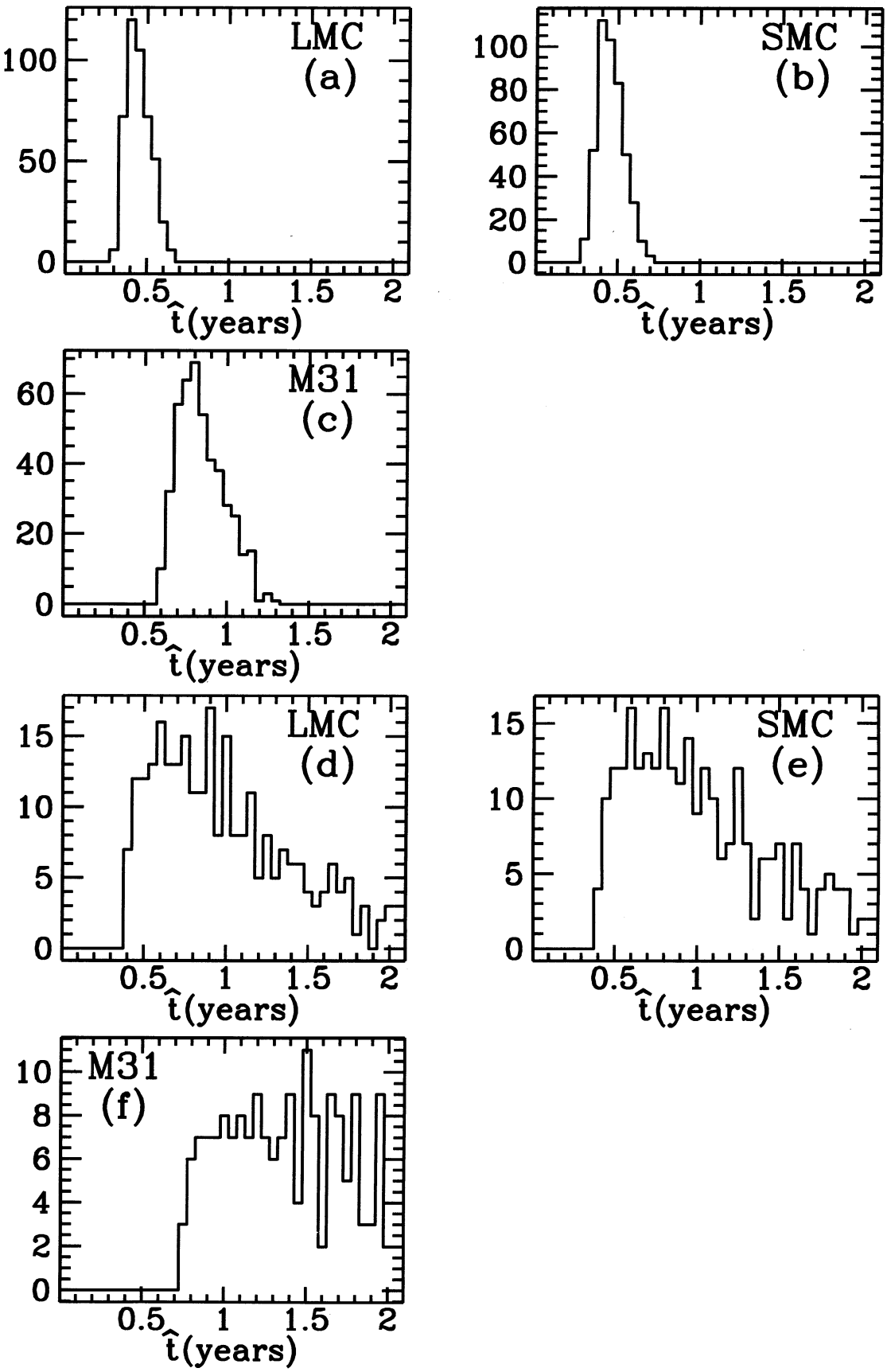

FIG. 1.—Histograms of the average duration $\langle \hat{t} \rangle = (4/\pi)\tau/\Gamma$ for the ensemble of halo models discussed in the text. Part (*a*) is for the LMC, (*b*) is for the SMC, and (*c*) is for M31. If optical depth tracked microlensing rate perfectly, each histogram would be a delta function. Parts (*d*)–(*f*) are the same for a maximal disk model. Note all plots are for $m = 1\ M_\odot$; scale by η_m^{-1} for other masses (eq. [3]).

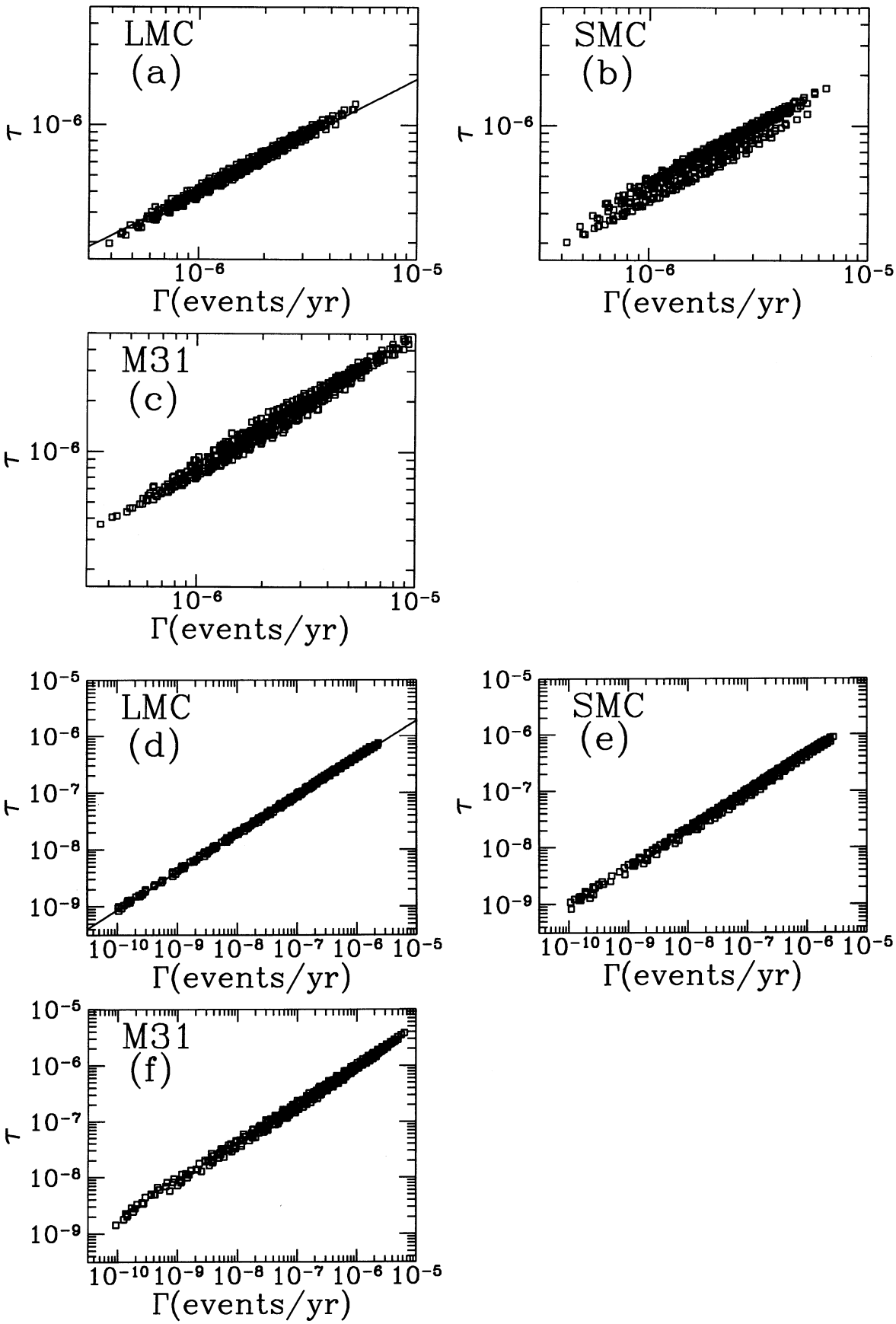

FIG. 2.—Scatter plots of microlensing rate vs. optical depth for the ensemble of models discussed in the text. Part (*a*) is for the LMC, (*b*) is for the SMS, and (*c*) is for M31. Each point represents a consistent model of the dark halo. Parts (*d*)–(*f*) are the same for a maximal disk model. All event rates scale $\Gamma \propto \eta_m$.

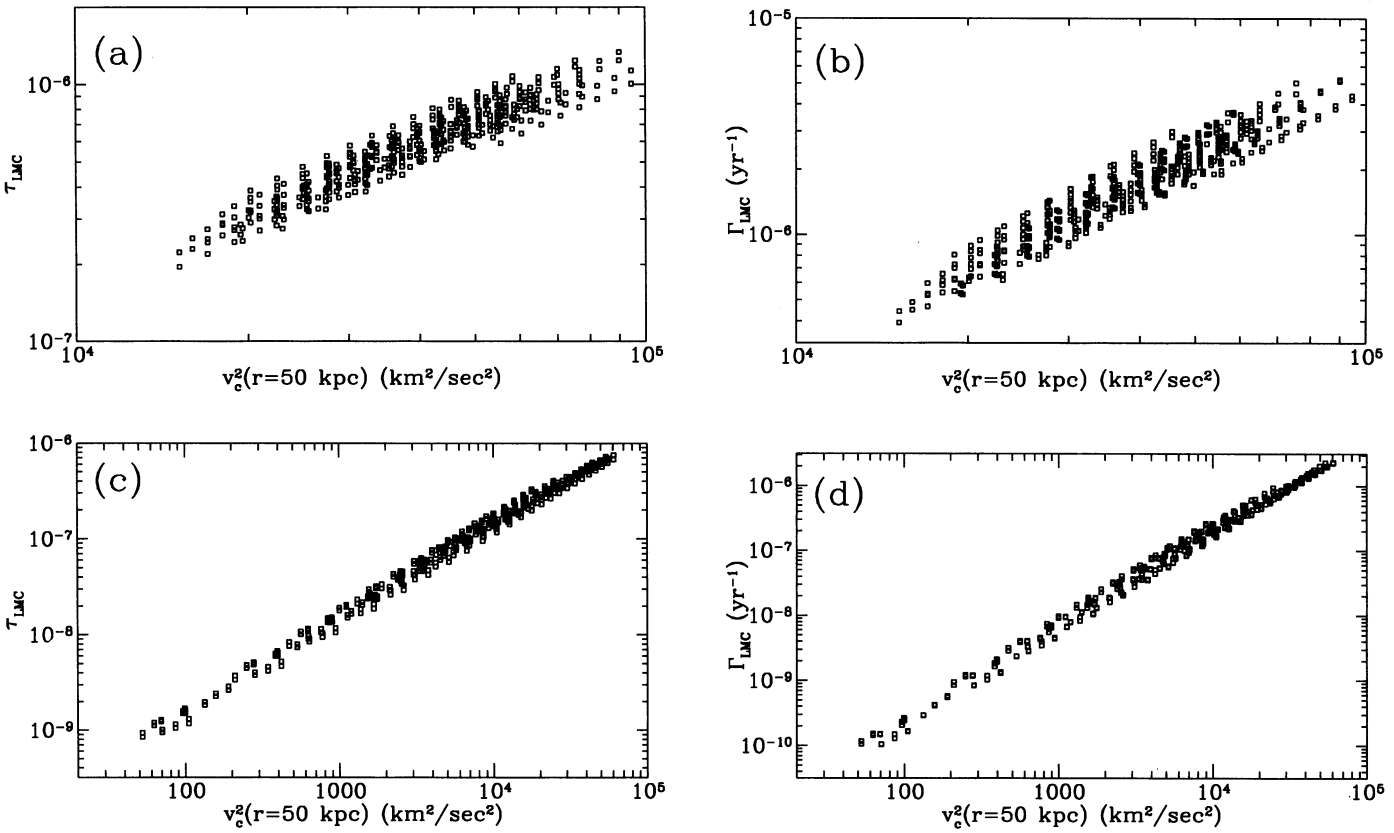

FIG. 3.—Scatter plots of optical depth vs. v_c^2(50 kpc), the square of the total rotation velocity at 50 kpc in the Galactic plane. The mass of the Galaxy interior to this distance is proportional to this squared velocity. Parts (*a*) and (*b*) are for a canonical disk, while parts (*c*) and (*d*) are for a maximal disk.

that $\langle \hat{t} \rangle$ is indeed much less model dependent than either τ or Γ. While the rate and τ vary by more than a factor of 10 in these plots, their ratio varies only ~ 2 for a canonical disk. In fact, we note that the line $\Gamma \propto \tau^{3/2}$ is a fairly good fit to all the models we have considered.[8] Thus the large scatter in $\langle \hat{t} \rangle$ seen in the maximal disk histograms is mostly just due to the large scatter in rate. (The rate varies more than the optical depth.) In all the plots we use $m = M_\odot$, but for an arbitrary mass distribution just scale Γ by η_m and $\langle \hat{t} \rangle$ by η_m^{-1}. Keep in mind that a given experiment can produce only one point in the Γ, τ plane and that the primary use of a measurement will be to find f, the MACHO fraction. We see that for approximate work, the optical depth does a reasonable job of predicting the rate. But for more detailed work, especially when efficiencies are involved, the difference between rate and optical depth should be kept in mind. We also note that the predicted distribution of event durations is found as a differential rate (Appendix B). Note that since the optical depth is independent of lens velocity and mass (apart from efficiencies), it is probably a more robust estimator of the total mass in MACHOs, while the rate (and duration distribution) depends upon the unknown lens mass distribution. However, the rate is more accurately determined from observations, since it is just the number of observed microlensing events divided by the total effective exposure in star-years, while the observed optical depth is this observed rate times the average event duration (modulo event detection efficiencies). Thus, while the observed rate is uncertain by at least the square root of the number of observed events, the optical depth has this uncertainty as well as the uncertainty in determining the average event duration. When ratios of rates or optical depths are used, some of the mass and velocity dependence may cancel out.

Next let us turn to the scatter in the predicted microlensing rate caused by uncertainties in the halo parameters. Figure 2 shows that for all lines of sight, there is a scatter in the rate of more than a factor of 10 for a canonical disk. For the LMC, the models with the smallest rate have spherical halos with small core radii, falling rotation curves, and small values of v_0, while the models with the largest rates have either spherical or flattened halos, but large core radii, rising rotation curves, and large values of v_0. This is as expected, since any model which puts more mass at a large distance in the direction of the LMC will have a larger microlensing rate and a larger optical depth. This is shown in Figure 3, in which we plot the optical depth against the rotation velocity at $r = 50$ kpc. The correlation between τ and $v_c^2(r = 50$ kpc), while not perfect, is quite good. Note that the mean value of the rotation velocity at R_0 is nearly independent of the microlensing rate. Figures 2*d*–2*f* and Figures 3*c*–3*d* show the case of a maximal disk. Here we see

[8] To the extent that the relation $\Gamma = a\eta_m f^{-1/2}\tau^{3/2}$ holds, where a is a constant from theory, we have that $a = f^{-1/2}\eta_m^{-1}(4/\pi)^{3/2}\langle \hat{t} \rangle^{-3/2}\Gamma^{-1/2}$ is independent of the model parameters. Thus, if the MACHO fraction f were known, one could extract the mass integral η_m from observables $\eta_m \approx f^{1/2}\, a^{-1}(4/\pi)^{3/2} N_{\rm eff} E^{1/2}\, (\Sigma t_i/\epsilon_i)^{-3/2}$, where E is the total exposure, $N_{\rm eff} = \Sigma \epsilon_i^{-1}$, ϵ_i is the efficiency at which events of duration t_i are recovered, and the sums go from 1 to the number of observed microlensing events. For LMC microlensing in our set of models, we find $a \approx 3850 \pm 260$ yr^{-1}. The physical basis for this relationship may simply be that the optical depth is proportional to the mass along the line of sight $\propto v_c^2$, and the rate is proportional to the optical depth times v_c.

that the rate and optical depth can be considerably smaller than for a canonical disk. Also, there is a variation between models of several orders of magnitude. This is as expected, since in these models the disk is the main contributor to the rotation curve at the solar distance. Thus, a smaller enclosed halo mass is required to match observations, and the halo parameters are poorly constrained.

The halo may only consist of a fraction f of baryonic matter in the form of MACHOs. Thus, a factor of more than 10 uncertainty in the predicted rate caused by the poorly determined halo parameters makes it difficult to determine the allowed amount of nonbaryonic dark matter. It is clearly essential to reduce the uncertainty.

5. REDUCING MODEL UNCERTAINTIES

The primary way of reducing the model uncertainties in the microlensing observables is to determine the halo parameters. Even within the restricted framework of the power-law galaxy models, if β, v_0, q, R_0, and R_c are known, there is still uncertainty in the rate. This is because the DFs (eq. [8]) are the simplest consistent with the potential and the density, but they are certainly not unique. There are still further DFs that depend on nonclassical third integrals of motion and generate anisotropic velocity distributions. Note, also, that even though our models give a plausible representation of the Milky Way, there certainly exist other alternatives (see, e.g., Frieman & Scoccimarro 1994; Gates & Turner 1993; Giudice, Mollerach, & Roulet 1994) with different lensing properties. And of course, the size of the disk plays a crucial role.

One obvious way to determine halo parameters is to use conventional astronomical techniques—observations of stars, gas, and satellites—to fix the solar radius and circular speed more accurately. For example, fixing the solar radius at 8 kpc, and demanding $v_{\rm circ} = 220$ km s^{-1} $\pm$ 5% between 8 and 16 kpc reduces the spread in microlensing rates toward the LMC from more than a factor of 10 to a little more than a factor of 2 (for the canonical disk). Uncertainties in τ and $\langle \hat{t} \rangle$ are reduced similarly. A better determination of the halo core radius by stellar observations would also be important.

However, it is also possible to use the microlensing experiments themselves to determine the halo parameters and reduce the model uncertainty. The basic idea is to exploit the fact that there are at least four viable lines of sight out of the Milky Way in which to measure the microlensing rate and average event duration. Each line of sight (LMC, SMC, M31, and the bulge) offers a different "pencil beam" through the dark halo, and so by comparing the rates, optical depths, and average durations among the different lines of sight, information concerning the halo shape can be gained. Several of the parameters, such as flattening q and asymptotic slope of the rotation law β, may best be determined this way. So microlensing gives us a new probe of the density and velocity structure of the dark halo. This is in addition to information on the size of the disk gained via microlensing.

For instance, a scatter plot of the ratio of LMC and SMC rates versus the LMC and SMC average durations is shown in Figure 4*a*. The models clearly fall into two distinct groups. Those models marked with a circle all have round halos (E0),

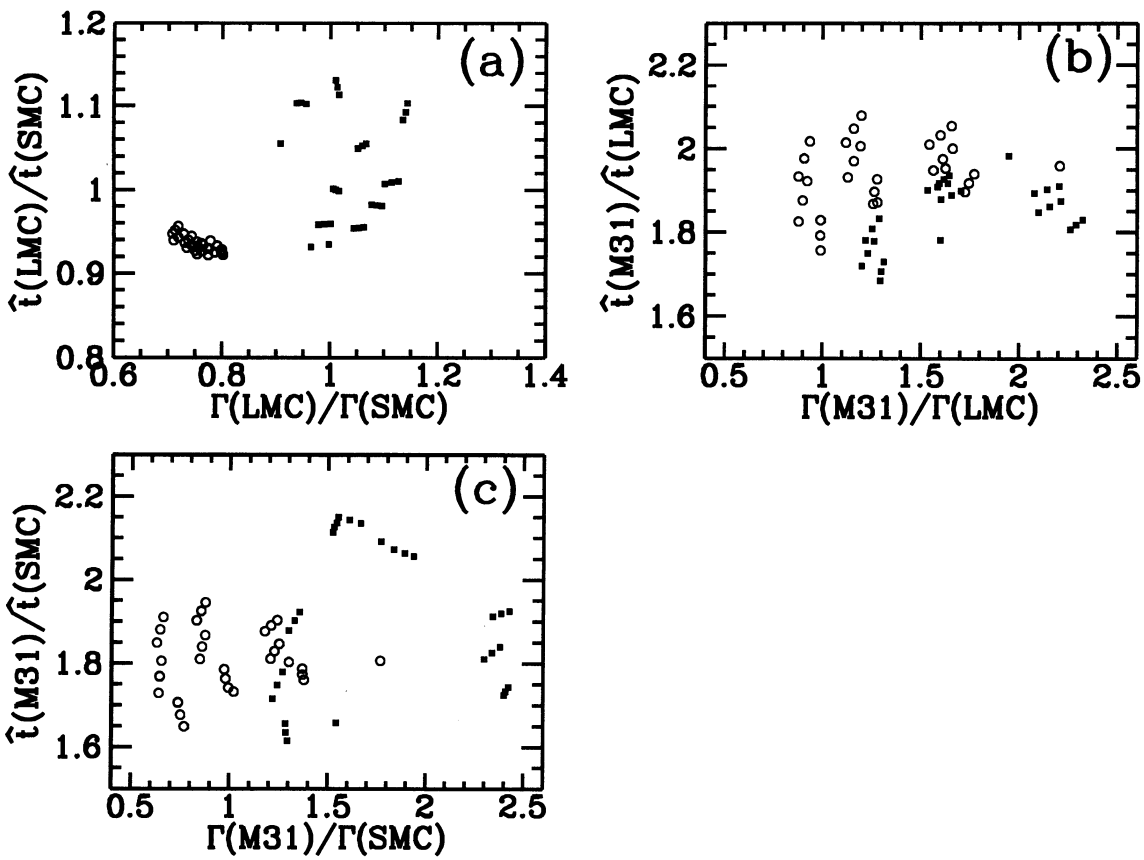

FIG. 4.—Finding the flattening parameter q. Scatter plots of the ratio of rates vs. the ratio of event durations. Circles represent halo models which are spherical ($q = 1$), while squares represent flattened halos ($q = 0.71$ for $\beta = 0, -0.1$; $q = 0.78$ for $\beta = 0.1$). Part (*a*) is for LMC/SMC and shows clear separation of spherical and flattened halos. Part (*b*) is M31/LMC, and part (*c*) is M31/SMC.

while those with a square are flattened to roughly E6. Thus the ratio of LMC rate to SMC rate is an excellent indicator of halo flattening. This effect was first discovered, using optical depth rather than microlensing rate, by Sackett & Gould (1993). Frieman & Scoccimarro (1994) have recently cautioned that the robustness of this diagnostic may be lost if the halo is tilted with respect to the disc, although such a configuration cannot be a long-lasting equilibrium. So, the halo flattening can probably be determined if enough events are found to allow accurate measurement of the SMC microlensing rate. Figures 4*b* and 4*c* show the rate ratio for M31/LMC and M31/SMC. While separation of flattened models is still evident, one sees from the figures that it is the LMC and SMC position relative to the halo axis of symmetry that make the measurement of the flattening so easy. Note again that in an experiment one measures only one LMC rate (and optical depth) and one SMC rate, and so one obtains only one point in any of these scatter plots. It is also interesting to observe from Figure 4*a* that the model uncertainties in the LMC/SMC rate ratio are much greater for flattened halos than for spherical halos. The case of a maximal disk is not shown, since it looks almost identical to Figure 4.

Can we use microlensing to determine whether the halo has a rising or falling rotation curve? The LMC and SMC are at nearly the same distances (50 and 60 kpc), so it is natural to expect the ratio of M31 to LMC microlensing to be the most useful discriminant. Note that rate ratios are convenient to use, because the magnitude of any rate always contains the unknown parameter f. In Figure 5 we plot the M31/LMC rate ratio versus the LMC rate for the set of models above, with triangles for $\beta = 0.2$ (falling rotation curve), circles for $\beta = 0$ (asymptotically flat rotation curves), and stars for $\beta = -0.2$ (rising rotation curve). In Figure 5*a*, all models are plotted, while in Figures 5*b* and 5*c* only models with spherical ($q = 1$) and flattened ($q = 0.71$ or $q = 0.78$) halos, respectively, are shown. In Figure 5*a* some separation of models with different values of β is evident, but there is substantial ambiguity, which would make a direct estimate of β using this method difficult. However, suppose that we have already determined the halo flattening by use of the ratio $\Gamma_{LMC}/\Gamma_{SMC}$. Then, as shown in Figures 5*b* and 5*c* for a canonical disk, a fairly clear separation of rising, falling, and flat rotation curve parameter can be accomplished. Thus, the ambiguity seen in Figure 5*a* is largely removed when models with different flattenings are plotted separately. The exception is some overlap between models with $R_c = 2$ kpc and $R_c = 20$ kpc and different values of β. This ambiguity is probably removable, as discussed below. The case of a maximal disk is not displayed because it is very similar. So the asymptotic form of the rotation law, or equivalently β, can probably be determined from the M31/LMC rate ratio once q is known. Keep in mind, however, the caveats mentioned in § 3 concerning our M31 rate calculation, which may result in cor-

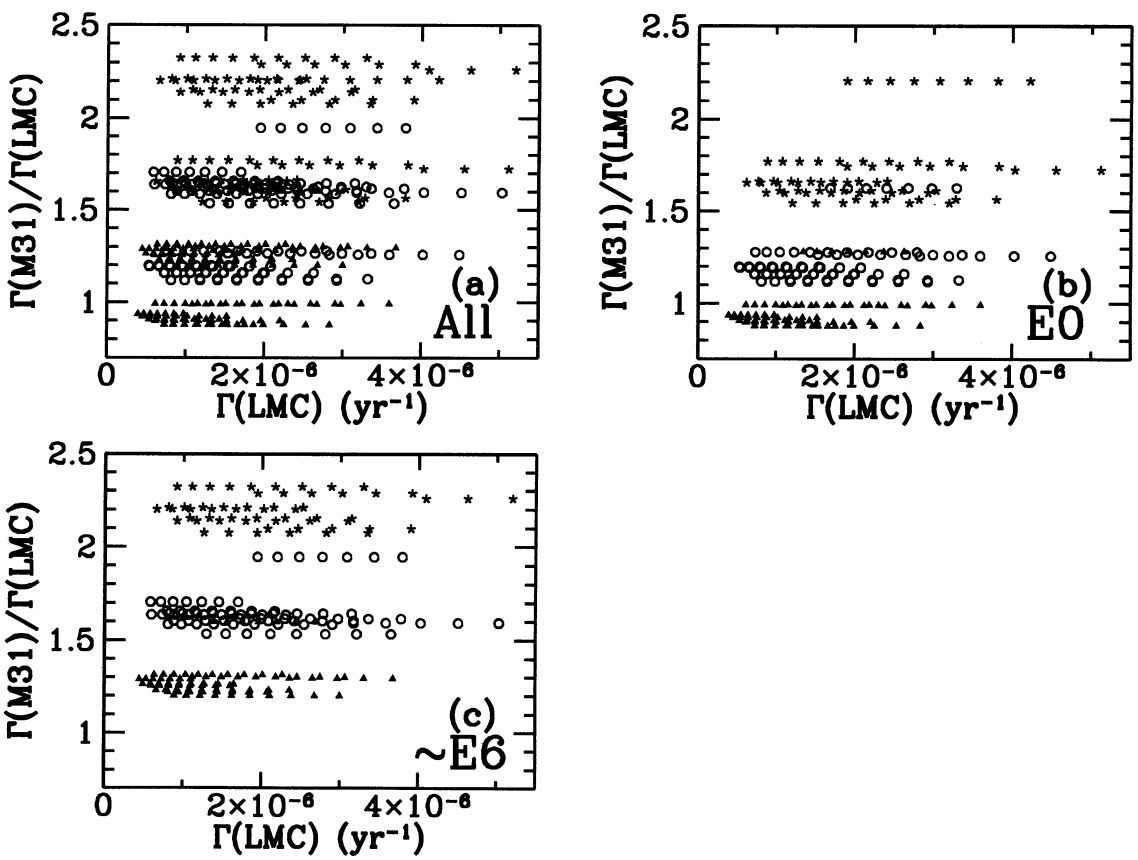

FIG. 5.—Finding the asymptotic slope β. Scatter plots of the M31 rate divided by the LMC rate vs. the LMC rate. Stars represent halo models with $\beta = -0.2$ (rising rotation curve), the circles represent models with $\beta = 0$ (flat), and triangles represent models with $\beta = 0.2$ (falling). Part (*a*) shows all models, while part (*b*) shows only spherical models and part (*c*) shows only the flattened models. Separation of the models becomes easier if the flattening is known. The line of ambiguity in some panels is due to $R_c = 20$ kpc models, which can be distinguished as shown in Fig. 6. All event rates scale $\Gamma \propto \eta_m$.

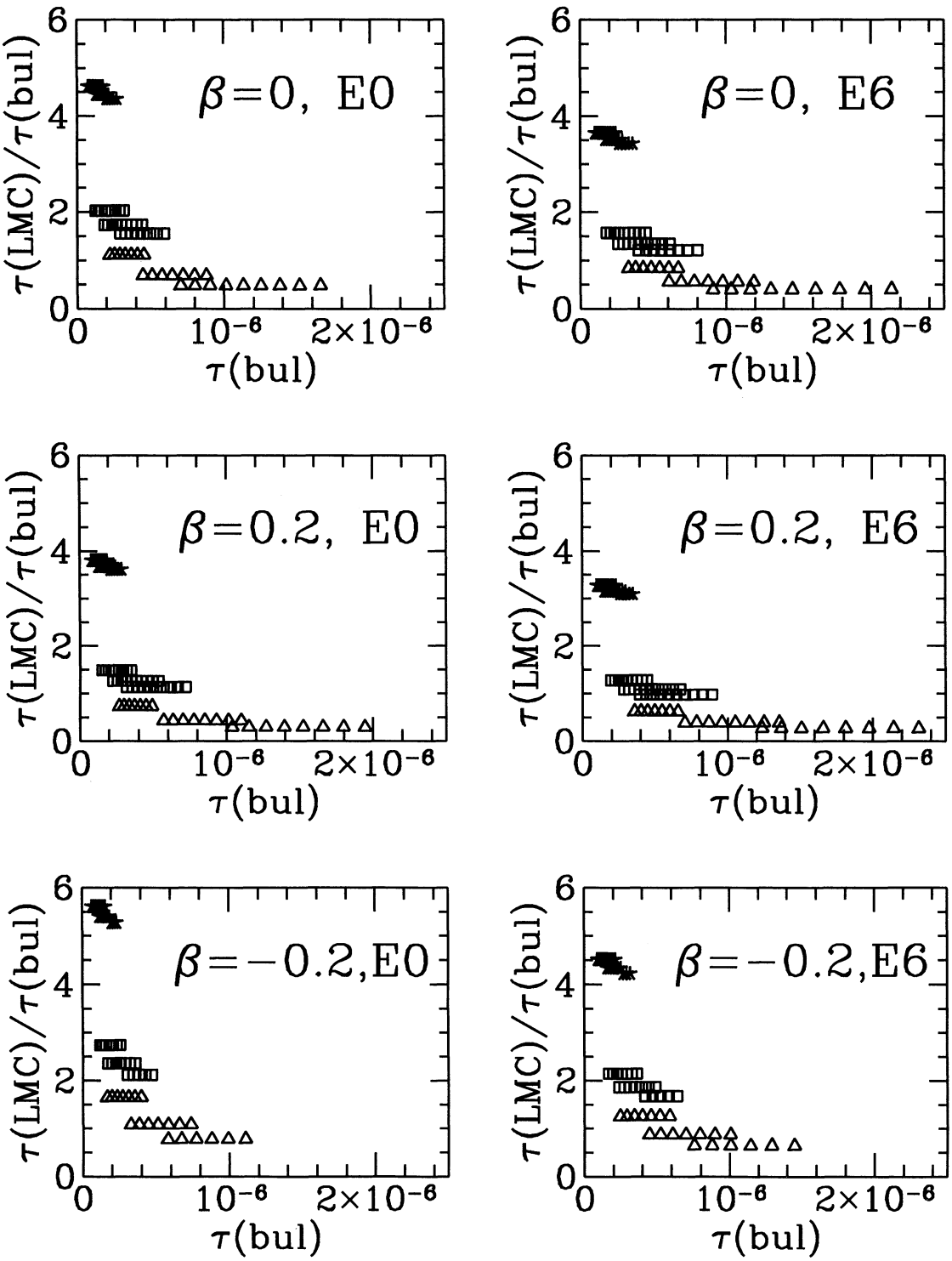

FIG. 6.—Finding the core radius R_c. Each panel shows models of definite values of β (rotation curve slope) and q (flattening). Separation between models is quite good. Triangles represent $R_c = 2$ kpc, squares represent $R_c = 5$ kpc, and stars represent $R_c = 10$ kpc. Panels marked E0 are for spherical halos, while those marked E6 are for flattened halos. Models with $R_c = 20$ kpc were also considered, but they are easily distinguished since they typically have $\tau(\mathrm{LMC})/\tau(\mathrm{bul}) > 10$ and therefore fall off the top of the figures.

rections which modify this effect. If halo microlensing can be distinguished from M31 microlensing, a measurement of β should then be possible.

Next, can we determine the halo core radius R_c? The parameter R_c affects mainly the inner portion of the halo and overall normalization of the halo mass. This overall normalization is mixed in with v_0 and f, and so the best hope in determining R_c is probably a comparison of the bulge with a more distant source such as the LMC. Here we have the problems mentioned in § 3 concerning bulge microlensing; our modeling of the distribution of velocities is not adequate along the disk. But the optical depth is independent of the velocities and will give some indication of the rate. Even so, our calculations do not give the total optical depth toward the bulge, merely the contribution of the optical depth from the halo.

In Figure 6, we plot the LMC/bulge optical depth ratio versus the bulge optical depth, where triangles indicate $R_c = 2$ kpc, boxes indicate $R_c = 5$ kpc, and stars indicate $R_c = 10$ kpc. A reasonably clean separation is obtained when this ratio is plotted for all the models (not shown). In Figure 6, this separation is made clear-cut, if one supposes β and q have already been measured by the methods above. The $R_c = 20$ kpc models have an LMC/bulge ratio of greater than 10 and are very easily distinguished even with no prior knowledge of β and q. (They fall off the top of the plots in Fig. 6.) Even if β and q are not known, the separation is quite good if the value of the solar radius R_0 is held fixed. So, a better determination of R_0 by nonmicrolensing means can allow a clearer separation of the effect of the halo core radius. The case of a maximal disk is not shown, since it gives very similar results.

6. DISTRIBUTION OF EVENT DURATIONS

Since the duration of a microlensing event is proportional to the Einstein radius ($\propto m^{1/2}$), the duration of an event gives information about the mass of lens which caused it. In trying to understand the nature of the objects responsible for the observed microlensing, this is important information. But the duration also depends upon the unknown lens velocity and distance. Thus, a given mass MACHO can cause a wide distribution of event durations. This distribution must be used statistically to infer probable masses from observed durations. Using the DFs (eq. [8]), the distribution of event durations can be found. The formula and definitions are given in Appendix B. In Figure 7, we show several $\hat{t}$ distributions. One sees that different halo parameters give quite different distributions. It is the average of these distributions $\langle \hat{t} \rangle$ that is shown in the histograms in Figure 1. Figure 7 shows that, as expected, uncertainty in the halo model will lead to additional uncertainty in determining the masses of the lensing objects. The curves labeled (a), (b), and (c) are canonical disk cases with various choices of halo parameters, while curve (d) shows a maximal disk example. We also note that the scaling introduced in Griest (1991) works fairly well for models we considered. That is, by scaling the $\hat{t}$ axis by $\langle \hat{t} \rangle^{-1}$, and the $d\Gamma/d\hat{t}$ axis by $\langle \hat{t} \rangle$, all the curves are found to lie roughly on top of each other. This means that for power-law galaxy models along a given line of sight, the shape of the distribution is much more model independent than peak value.

In a future paper, we plan to explore further the information that can be extracted from event duration distributions and include other possibilities such as triaxiality, streaming motion, etc.

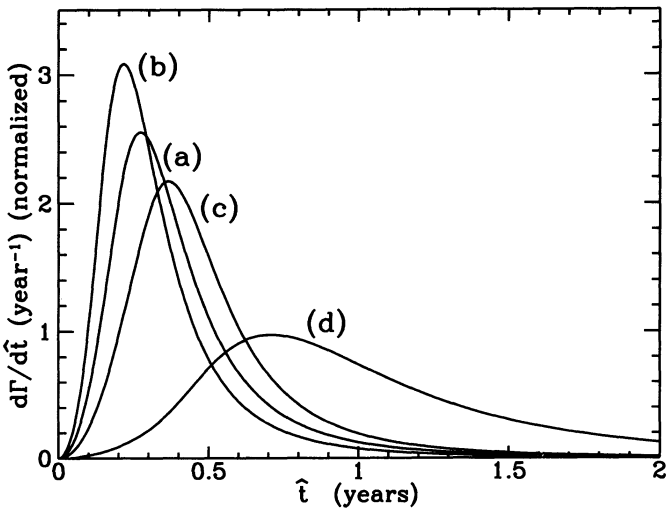

FIG. 7.—Examples of LMC $\hat{t}$ distributions for various model parameters. The integral under each distribution is unity. The curve marked (*a*) is for a "standard" spherical halo ($\beta = 0$, $q = 1$, $R_c = 5$ kpc, $v_0 = 200$ km s^{-1}, $R_0 = 8.5$ kpc, and $\Gamma = 1.64 \times 10^{-6}$ events yr^{-1}). Curve (*b*) has a shorter average duration ($\beta = -0.2$, $q = 1$, $R_c = 5$ kpc, $v_0 = 200$ km s^{-1}, $R_0 = 8.5$ kpc, and $\Gamma = 3.9 \times 10^{-6}$ events yr^{-1}). Curve (*c*) has a longer average duration ($\beta = 0.2$, $q = 0.78$, $R_c = 10$ kpc, $v_0 = 210$ km s^{-1}, $R_0 = 8.5$ kpc, and $\Gamma = 1.24 \times 10^{-6}$ events yr^{-1}). Finally, curve (*d*) has a maximal disk, which greatly reduces the amount of halo material ($\beta = 0$, $q = 1$, $R_c = 20$ kpc, $v_0 = 90$ km s^{-1}, $R_0 = 7$ kpc, and $\Gamma = 9.37 \times 10^{-8}$ events yr^{-1}). The average of each distribution is $\langle \hat{t} \rangle$. All event rates scale $\Gamma \propto \eta_m$.

7. CONCLUSIONS

This paper has shown how to exploit the power-law galaxy models (E93, E94) as simple, flexible, and realistic representations of the dark halo. These models have the advantage of simple and analytic phase space distribution functions and therefore permit accurate calculation of the optical depth, microlensing rate, and average event duration. We provide formulae for these quantities as a function of the halo parameters and source distance and direction (Appendix A). The distribution of event timescales is presented in Appendix B. We apply our formulae to study microlensing toward the Large and Small Magellanic Clouds (LMC and SMC), the Galactic bulge, and the M31 disk galaxy. We find that:

1. For a canonical disk, the optical depth is a reasonable indicator of the microlensing rate to within a factor of 2. This is important because the optical depth is much easier to calculate than the rate and probably will continue to be widely used by investigators. For more accurate work, as well as for derivations of the distribution of durations, galaxy modeling with distribution functions is crucial. For a maximal disk, the agreement between optical depth and rate is less robust, though the relation $\Gamma \propto m^{-1/2}\tau^{3/2}$ seems to hold.

2. The evaluation of the fraction f of the halo consisting of MACHOs is hampered by the uncertainties in the galactic constants, such as the shape of the rotation law and the flattening of the dark halo. For a realistic set of halo models, we found rates toward the LMC and SMC can vary by more than a factor of 10 from model to model for a canonical disk, and by several orders of magnitude for a maximal disk. Left unaddressed, this model uncertainty will thwart accurate determination of f.

3. An attractive way of reducing the uncertainty—which simultaneously opens up a new method in galactic

astronomy—is to use microlensing to explore the shape and structure of the dark halo. This has also been realized by Sackett & Gould (1993), who showed that the ratios of optical depth toward the LMC and SMC are a robust indicator of the flattening of the dark halo. We confirm this result by showing that the ratios of the event rates also distinguish flatness. In particular, the ratio of microlensing rates toward the LMC and SMC is ~ 0.7–0.8 for E0 halos and ~ 1.0–1.2 for E7 halos. This is true for both canonical and maximal disk models. Once the flattening has been established, the asymptotic slope of the rotation curve β might be determined using the M31/LMC rate ratio. The LMC/bulge ratio contains important information on the halo core radius. We caution that this may not be easy to extract, since the dark halo is probably not the dominant source of lenses toward the bulge.

In summary, the discovery of a dark halo consisting of a significant fraction of MACHOs is only the starting point for an exploration of the halo characteristics which microlensing can help determine.

K. G. thanks A. Gould, D. A. Merritt, and D. N. Spergel for help in the early stages of this project. K. G. acknowledges a DOE OJI grant, and K. G. and C. W. S. thank the Sloan Foundation for their support. Work performed at Lawrence Livermore National Laboratory is supported by the DOE under contract W7405-ENG-48. Work performed by the Center for Particle Astrophysics on the University of California campuses is supported in part by the Office of Science and Technology Centers of NSF under cooperative agreement AST 88-09616. Work performed at Mount Stromlo and Siding Spring Observatories is supported by the Bilateral Science and Technology Program of the Australian Department of Industry, Technology and Regional Devlopment.

APPENDIX A

In this appendix, we give the formulae for the microlensing rate and optical depth for the general flattened halo model described in the text (eqs. [4]–[7]). The total rate Γ of microlensing in a power-law halo with model parameters β, v_0, R_c, R_0, and q is

$$\Gamma = \frac{C_0 u_T}{\sqrt{2\pi M/M_\odot}} \frac{v_0^3 R_c^{3\beta/2}(\beta+2)(1-q^2)}{2cq^2\sqrt{-\beta}L^{1/2+3\beta/2}} \frac{\Gamma(n_\beta)}{\Gamma(d_\beta)} I_1 + \frac{C_0 u_T}{\sqrt{2\pi M/M_\odot}} \frac{v_0^3 R_c^{2+3\beta/2}(\beta+2)}{cq^2\sqrt{-\beta}L^{5/2+3\beta/2}} \frac{\Gamma(n_\beta)}{\Gamma(d_\beta)} I_2 + \frac{C_0 u_T}{\sqrt{2\pi M/M_\odot}} \frac{v_0^3 R_c^{3\beta/2}[2-(1+\beta)/q^2]}{c\sqrt{-\beta}\,L^{1/2+3\beta/2}} \frac{\Gamma(n_\beta - 2/|\beta|)}{\Gamma(d_\beta - 2/|\beta|)} I_3 . \tag{A1}$$

Here $C_0 = 1/(GM_\odot)^{1/2}$, $\Gamma(x)$ is the gamma function, and the integrals I_i are

$$I_1 = \int_0^1 \frac{ds\sqrt{s(1-s)}(A's^2 + B's + C')}{(D's^2 + Es' + F')^{2+3\beta/2}} ,$$

$$I_2 = \int_0^1 \frac{ds\sqrt{s(1-s)}}{(D's^2 + Es' + F')^{2+3\beta/4}} , \tag{A2}$$

$$I_3 = \int_0^1 \frac{ds\sqrt{s(1-s)}}{(D's^2 + Es' + F')^{1+3\beta/4}} ,$$

with

$$A' = 3\cos^2 b , \quad B' = -6R_0 \cos b(\cos l)/L , \quad C' = 2R_0^2/L^2 + R_0^2(\cos^2 l)/L^2 + R_0^2 \sin^2 l(\sin^2 b)/L^2 ,$$
$$D' = \cos^2 b + q^{-2}\sin^2 b , \quad E' = -2R_0 \cos b(\cos l)/L , \quad F' = (R_c^2 + R_0^2)/L^2 . \tag{A3}$$

The quantities b, l are the galactic coordinates of the source star, L is the source distance, G is Newton's constant, and c is the speed of light. The constants n_β and d_β have a different form according to whether β is positive or negative:

$$n_\beta = \begin{cases} \dfrac{-4}{\beta} - \dfrac{3}{2} , & \text{if } \beta < 0 , \\ \dfrac{4}{\beta} + 2 , & \text{if } \beta > 0 , \end{cases} \tag{A4}$$

$$d_\beta = \begin{cases} \dfrac{-4}{\beta} - 1 , & \text{if } \beta < 0 , \\ \dfrac{4}{\beta} + \dfrac{5}{2} , & \text{if } \beta > 0 . \end{cases} \tag{A5}$$

In the limit $\beta \to 0$ (the case of an asymptotically flat rotation curve), the expression for the rate follows from the above by systematic use of the formula $\Gamma(x + \frac{1}{2})/\Gamma(x) \to x^{1/2}$ as $x \to \infty$. The optical depth τ is

$$\tau = \frac{v_0^2 R_c^\beta u_T^2}{c^2 q^2 L^\beta} \int_0^1 \frac{s(1-s)(A''s^2 + B''s + C'')ds}{(D's^2 + E's + F')^{(\beta+4)/2}}, \tag{A6}$$

where

$$A'' = (1 - \beta q^2)\cos^2 b + [2 - (1+\beta)q^{-2}]\sin^2 b, \qquad B'' = -2(1-\beta q^2)R_0 \cos b(\cos l)/L,$$
$$C'' = [R_c^2(1 + 2q^2) + R_0^2(1 - \beta q^2)]/L^2. \tag{A7}$$

The quadratures are straightforward to evaluate on the computer.

APPENDIX B

The distribution of event durations is important for finding the mass of the lensing objects. It is given by the normalized differential microlensing rate $(d\Gamma/d\hat{t})/\Gamma$, where $\hat{t} = 2R_e/v_\perp$, and $v_\perp$ is the speed of the MACHO perpendicular to the line of sight. The time the MACHO spends inside the Einstein radius, $t_e = (u_T^2 - u_{\min}^2)^{1/2}\hat{t}$, where $u_{\min}$ is defined in equation (1), and $u_T = 1$. The average duration is related to the average $\hat{t}$ by $\langle t_e \rangle = (\pi/4)\langle \hat{t} \rangle$. In many cases, it is advantageous to use distributions in $\hat{t}$, since they are independent of the amplifications.

For the model described in the text, we find:

$$\frac{d\Gamma}{d\hat{t}} = 8\frac{u_T}{\pi c^2}\left(\frac{L^6}{R_C^4 \hat{t}^4}\right)(\beta+2)|\beta|^{1+4/\beta}(q^{-2}-1)(a_1 G' J_1 + a_2 H' J_2)$$
$$+ 8\frac{u_T}{\pi c^2}\left(\frac{L^4}{R_c^2 \hat{t}^4}\right)\frac{|\beta|^{1+4/\beta}(\beta+2)}{q^2} a_1 J_1 + 8\frac{u_T}{\pi c^2}\left(\frac{L^4}{R_c^2 \hat{t}^4}\right)|\beta|^{1+2/\beta}[2 - q^{-2}(1+\beta)]a_3 J_3, \tag{B1}$$

where

$$a_1 = \begin{cases} -1 - (4/\beta), & \beta < 0, \\ 1 + (4/\beta), & \beta > 0, \end{cases}$$
$$a_2 = \frac{4(\beta+4)}{\beta^2}, \tag{B2}$$
$$a_3 = \begin{cases} -1 - (2/\beta), & \beta < 0, \\ 1 + (2/\beta), & \beta > 0 \end{cases}$$

and the integrals J_i are

$$J_1 = \int ds\, s^2(1-s)^2 \left| \frac{K'}{g_1(D's^2 + E's + F')^{\beta/2}} - \frac{H'}{g_1} s(1-s) \right|^{4/\beta},$$
$$J_2 = \int ds\, s^3(1-s)^3 \left\{ \frac{A'}{3} s^2 + \frac{B'}{3} s + \left[C' - 2\left(\frac{R_0}{L}\right)^2 \right] \right\} \left| \frac{K'}{g_2(D's^2 + E's + F')^{\beta/2}} - \frac{H'}{g_2} s(1-s) \right|^{4/\beta - 1}, \tag{B3}$$
$$J_3 = \int ds\, s^2(1-s)^2 \left| \frac{K'}{g_3(D's^2 + E's + F')^{\beta/2}} - \frac{H'}{g_3} s(1-s) \right|^{2/\beta}.$$

If $\beta < 0$, the integrals are evaluated over the interval $[0, 1]$. If $\beta > 0$, then we must restrict the domain of integration by

$$\hat{t}^2 \geq \frac{8\beta L s(1-s)(m/M_\odot)(D's^2 + E's + F')^{\beta/2}}{(v_0 c C_0)^2 (R_C/L)^\beta}. \tag{B4}$$

The constants A', B', C', D', and E' are given in Appendix A. The additional constants are

$$G' = \left(\frac{R_0}{L}\cos b \sin l\right)^2, \qquad H' = \frac{8}{L(cC_0)^2}\frac{m}{M_\odot},$$
$$K' = \left(\frac{v_0 \hat{t}}{L}\right)^2 \frac{1}{\beta}\left(\frac{R_C}{L}\right)^\beta, \qquad g_1 = H'^{(-\beta/4)}\left(\frac{v_0 \hat{t}}{L}\right)^2, \tag{B5}$$
$$g_2 = H'^{[\beta/(\beta-4)]}\left(\frac{L}{v_0 \hat{t}}\right)^{8/(\beta-4)}, \qquad g_3 = H'^{(-\beta/2)}\left(\frac{v_0 \hat{t}}{L}\right)^2.$$

REFERENCES

Alcock, C., et al. 1993, Nature, 365, 621
———. 1995, ApJ, 445, 000
Ashman, K. 1992, PASP, 104, 1109
Aubourg, E., et al. 1993, Nature, 365, 623
Bahcall, J. 1984, ApJ, 287, 926
Bahcall, J., Schmidt, M., & Soneira, R. 1983, ApJ, 265, 730
Baillon, P., Bouquet, A., Giraud-Heraud, Y., & Kaplan, J. 1993, A&A, 277, 1
Binney, J., & Tremaine, S. 1987, Galactic Dynamics (Princeton: Princeton Univ. Press)
Buchhorn, M. 1992, Ph.D. thesis, Australian National University
Caldwell, J. A. R., & Ostriker, J. P. 1981, ApJ, 251, 61
Crotts, A. P. S. 1992, ApJ, 399, L43
DeRejula, A., Jetzer, Ph., & Masso, E. 1991, MNRAS, 250, 348
Dubinski, J., & Carlberg, R. 1991, ApJ, 378, 496
Evans, N. W. 1993, MNRAS, 260, 191 (E93)
———. 1994, MNRAS, 267, 333 (E94)
Evans, N. W., & Jijina, J. 1994, MNRAS, 267, L21
Fich, M., & Tremaine, S. 1991, ARA&A, 29, 409
Fich, M., Blitz, L., & Stark, A. A. 1989, ApJ, 342, 272
Freeman, K. C. 1970, ApJ, 160, 811
Frieman, J., & Scoccimarro, R. 1994, ApJ, 431, L23
Gates, E., & Turner, M. S. 1993, preprint FERMILAB-Pub-93/357-A
Gilmore, G., Wyse, R. F. G., & Kuijken, K. 1989, ARA&A, 72, 555
Giudice, G. F., Mollerach, S., & Roulet, E. 1994, Phys. Rev. D, 50, 2406
Gould, A. 1990, MNRAS, 244, 25
———. 1993a, private communication
———. 1993b, ApJ, 404, 451
Griest, K. 1991, ApJ, 366, 412
Griest, K., et al. 1991, ApJ, 372, L79
Jetzer, Ph. 1991, Zurich Univ. Preprint ZU-TH 15/91
Jetzer, Ph., & Masso, E. 1994, Phys. Lett. B., 323, 347
Jones, B., et al. 1993, Lick preprint
Katz, N. 1991, ApJ, 368, 325
Kent, S. M. 1992, ApJ, 387, 181
Kerr, F. J., & Lynden-Bell, D. 1986, MNRAS, 221, 1023
Kiraga, M., & Paczyński, B. 1994, ApJ, 430, L101
Kuijken, K., & Gilmore, G. 1989, MNRAS, 239, 605
———. 1991, ApJ, 367, L69
Merrifield, M. R. 1992, AJ, 103, 1552
Nemiroff, R. J. 1991, A&A, 247, 73
Oort, J. H. 1960, Bull. Astron. Inst. Netherlands, 6, 249
Paczyński, B. 1986, ApJ, 304, 1
———. 1991, ApJ, 371, L63
Paczyński, B., et al. 1994, ApJ, 435, L113
Primack, J. R., Seckel, D., & Sadoulet, B. 1988, Ann. Rev. Nucl. Sci., 38, 751
Reid, N. J. 1989, in IAU Symposium No. 136, The Center of the Galaxy, ed. M. Morris (Dordrecht: Kluwer)
Rohlfs, K., Chini, R., Wink, J. E., & Bohme, R. 1986, A&A, 158, 181
Sackett, P. D., & Gould, A. 1993, ApJ, 419, 648
Sahu, K. 1994, Nature, 370, 275
Udalski, A., et al. 1993, Acta Astron., 43, 289
———. 1994a, ApJ, 426, L69
———. 1994b, Acta Astron., 44, 165
Warren, M. S., et al. 1992, ApJ, 339, 405
Zhao, H. S., Spergel, D. N., & Rich, R. M. 1995, ApJ, 440, L13